agriculture

MDPI

Article

Working Performance of the Low-Adhesion and Anti-Slip Bionic Press Roller in the Rice–Wheat Rotation Area

Hongjun Liu, Wei Yan, Yao Ji * and Wenyi Zhang

Nanjing Institute of Agricultural Mechanization, Ministry of Agriculture and Rural Affairs, Nanjing 210014, China; liuhongjun@caas.cn (H.L.); yanwei@caas.cn (W.Y.); zhangwenyi@caas.cn (W.Z.)
* Correspondence: jiyao@caas.cn

Abstract: During the working process of a conventional press roller in the rice–wheat rotation area, the phenomenon of soil adhesion and a large slip rate, which are directly related to the growth and the output of the wheat, occurred widely. It was found that the geometric structure of the back surface was one of the key reasons for *Carabus formosus nili* exhibiting low adhesion against the soil. In this paper, lessons are drawn from the non-smooth morphology theory and bionics principle. The bionic press rollers with bionically convex hull structures were designed after learning from the geometric structure of *Carabus formosus nili*, which modifies the geometric structure of the conventional press roller. The three-dimensional simulation model of a bionic press roller and soil was constructed in the ANSYS/LS-DYNA software(ANSYS, Canonsburg, PA, USA) to simulate the dynamic process of the interaction between the bionic roller and soil and to verify the rationality of the design of the bionic press roller. Based on the simulation of the interaction between the bionic press roller and the soil, the main factors affecting the bionic roller were determined: forward speed, load, and structural parameters. The field tests were carried out, and the orthogonal test was used to investigate the effects of forward speed, load, and structural parameters on the operation performance of the bionic press roller. Through the orthogonal test, the primary and secondary order of forward speed, load, and axial spacing were obtained. The optimal combination was: forward speed 7 km/h, load 400 N, and axial spacing 40 mm. This study provides a new idea and reference for the design of a press roller for wheat sowing in the rice–wheat rotation area.

Keywords: *Carabus formosus nili*; bionic; low-adhesion and anti-slip; press roller; finite element

Citation: Liu, H.; Yan, W.; Ji, Y.; Zhang, W. Working Performance of the Low-Adhesion and Anti-Slip Bionic Press Roller in the Rice–Wheat Rotation Area. *Agriculture* **2022**, *12*, 750. https://doi.org/10.3390/agriculture12060750

Academic Editor: Jacopo Bacenetti

Received: 30 March 2022
Accepted: 23 May 2022
Published: 25 May 2022

1. Introduction

A press roller is an important working part of a wheat planter in the rice–wheat rotation area in southern China [1–3]. However, there are few types of press rollers popularized and applied in this area at this stage [4]. In this case, the conventional press roller, which has a smooth surface, is the most common type of press roller, and the operational quality meets the requirements of the crops. During the operation, the surface is easy to adhere, and the pressing roller slides. After the operation, the seed depth is uneven, the contact between the seeds and the soil is insufficient, and the soil easily loses moisture, which seriously affects the growth of seedlings before winter and the lodging resistance of wheat seedlings in the later stage. Therefore, it is urgent to develop a new type of press roller for wheat sowing to realize a high quality, solve the above problems, and allow for an efficient mechanized production of wheat in the rice–wheat rotation area.

Different types of press rollers are used for soil compaction after sowing, such as cylindrical, rubber, and V-type press rollers [5,6]. These press rollers have advantages and disadvantages in terms of production costs, power consumption, soil adhesion, and slippage. The cylindrical press rollers have more uniform pressure distributions, lower manufacturing costs, and longer operation times than the other types of press rollers. However, when working in the rice–wheat rotation area with paddy soil, the surface

adhesion and roller slip phenomenon of these rollers are serious. The working performances of these press rollers are affected by many factors, such as the operation parameters (forward speed and load) [7,8], structural parameters (diameter and width) [9,10], geometry of the press roller, and soil parameters (moisture, shear strength, and cone index) [11–14]. Except for the soil parameters, the other factors are controllable. Meanwhile, without changing the geometric shape of the press roller, the performance improvement is limited.

In recent years, in order to improve the compaction quality after sowing, based on the conventional press roller, researchers have continued to innovate and optimize the structures of press rollers, which have four main structural forms: (1) a flexible bulge structure. Based on the flexible geometry features of the typical soil animal body surface, Jia et al. designed a profiling elastic press roller that could reduce the soil adhesion quality by more than 37.62% [15]; (2) a polyhedral geometric structure. Inspired by the geometric structure of the cuticle surface of a pangolin (*Manis Pentadactyla*), Zhang designed three bionically polyhedral geometrically structured press rollers that could avoid the hilling phenomenon [16]; (3) a ridged geometric structure. Inspired by the geometric structure of the dung beetle ventral surface, Tong designed a press roller with a bionically ridged structure that could reduce the drag force by 11.75~39.40% more than a conventional roller [17]; and (4) a convex hull geometric structure. Inspired by the geometric structure of a dung beetle head surface, Chang designed a bionic press roller based on the bionic convex geometric structure, which reduces the drag rate by between 6.59% and 36.94% and reduces the viscosity rate by between 26.68% and 35.13% in high-humidity soil conditions [18]. To sum up, the viscosity-reducing and slip-reducing structures, for which design inspiration mostly came from the biological surface, are the key to improving the performance of conventional pressing rollers, and the bionic convex geometry is an ideal object for high-humidity soil conditions [19,20].

In the past, to adapt to the working environment, soil conditions, and crop planting mode, researchers developed various types of press rollers. However, there is a lack of documentation on the press roller for the rice–wheat rotation area. This study develops a new bionic press roller by the bionic model in order to solve the problems of serious soil adhesion and high slip rate when the conventional press roller was working in the rice–wheat rotation area. The roller–soil interaction was established using the ANSYS/LS-DYNA software to simulate the dynamic soil behavior and the dynamic mechanical roller behavior. The orthogonal optimization methodology was adopted to optimize the structural and operating parameters to obtain the best working performance parameters. Then, the bionic ridged press roller was compared to verify the low-adhesion and anti-slip characteristics of the designed bionic press roller. The results can provide a theoretical basis and design basis for the research on low-adhesion and anti-slip press rollers.

2. Materials and Methods

2.1. Design of Bionic Press Roller

2.1.1. Design of Bionic Convex Hull

Figure 1a shows a *Carabus formosus nili*, the convex hull and surface morphological characteristics of which are low-adhesion and anti-slip while contacting with soil [21]. The convex hull has a narrow front and a gradually enlarged middle and back, which is close to the form of a long egg, and is generally 1~3 mm long and 1~4 mm wide, as shown in Figure 1a.

The *Carabus formosus nili* in the field in Northwest China was collected by the method of light lure and night search and was used as a test sample. Before the test, the samples were cleaned and disinfected with clean water, ethanol, and distilled water, and then the imaging agent was evenly sprayed on the surface of the beetle. The sample was scanned with a high-precision three-dimensional scanner (accuracy of 0.01 mm) to obtain a complete original 3D cloud point model. The reverse engineering software Geomagic Studio(Geomagic Inc., Morrisville, NC, USA) was used to process the 3D cloud point data,

and the entire geometric model was denoised and smoothed to obtain a smooth surface model (Figure 1b).

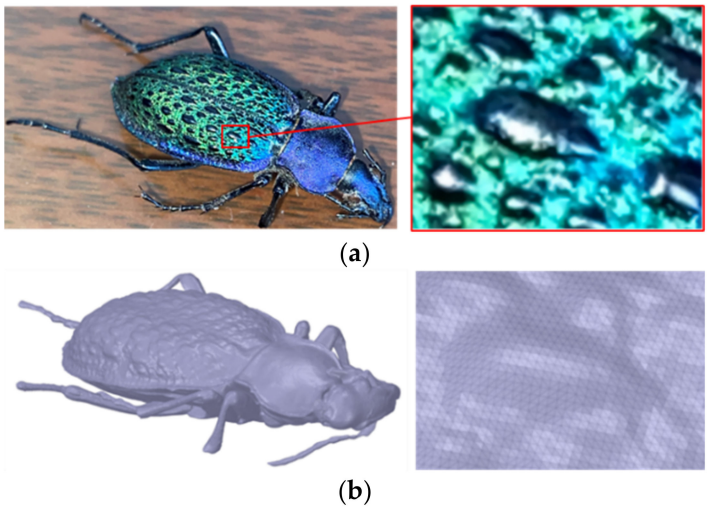

Figure 1. Geometric model of *Carabus formosus nili* and back convex hull:(**a**) real model and partial enlargement;(**b**) 3D reconstruction model and partial enlargement.

The smooth surface model was reconstructed in 3D by SolidWorks2018 software (SolidWorks, Waltham, MA), and the convex hull geometric surface was extracted. Then, with the design principle that the farthest normal phase distance of the convex package from the surface of the press roller was 16 mm and the proportional method in bionic design, the geometric convex package structure of the convex package on the back of *Carabus formosus nili* was designed, corresponding to the 3D model, as shown in Figure 2.

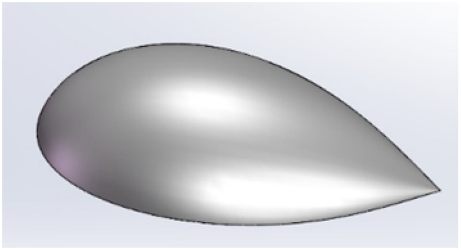

Figure 2. Structure diagram of bionic convex hull.

2.1.2. Layout Quantity of Convex Hull in the Base Plane

During operation, the press roller rolls simply, and the movement track of its edge line is a trochoid, as shown in Figure 3. The maximum radial distance between the convex hull and the axis center is point *a*, and Figure 3 shows the state diagram after point *a* rotates angle θ.

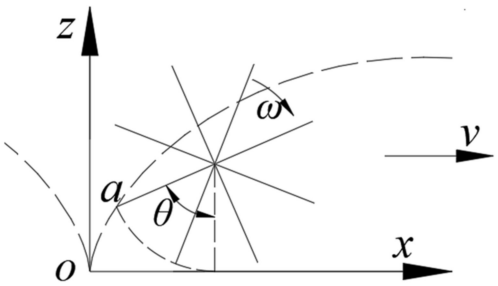

Figure 3. Schematic diagram of convex hull movement in soil.

Based on the relative positional relationship in Figure 3, the equation of motion for point a is determined to be

$$\begin{cases} x = R\theta - R\sin\theta \\ y = R - R\cos\theta \end{cases} \quad (1)$$

where R is the press convex roller radius, x is the x-axis coordinate value of the point a, and y is the y-axis coordinate value of the point a.

According to Equation (1) combined with the basic size of the press roller, the motion trajectory diagram was drawn and shown in Figure 4.

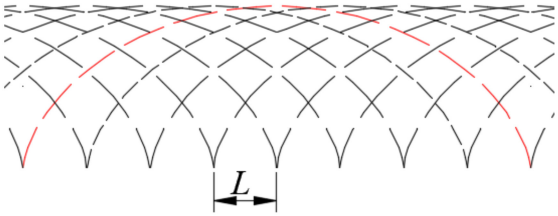

Figure 4. Definition of tine trajectory and parameters.

From Equation (1), it can be seen that the lateral displacement of one revolution ($\theta = 2\ \pi$) around the axis at point a is $2\pi R$.

The radial angle is $\theta_1 = 2\pi/n$ if it is evenly and equally arranged at the edge point, and n is the number of convex hulls. The circumference corresponding L to the edge points of the adjacent θ_2 is $R\theta_2$. The corresponding length L is as follows:

$$L = R\theta_2 = \frac{2\pi R}{n} \quad (2)$$

As can be seen in Figure 4 and Equation (2), the larger n is, the smaller L is, the larger the number of corresponding arrangements is, while the smaller n is, the larger L is, and the operation effect is not obvious. In this study, eight convex hulls were arranged on each radial base surface.

2.1.3. Axial Adjacent Convex Hull Phase Angle

After determining the number of convex hulls arranged on the radial base plane, it is necessary to determine the dislocation angle of the axial adjacent base planes. Taking 45° as a reference, the reference is divided into n_1 equal parts, and the dislocation angle θ_1 is $45°/n_1$. The shaded part in the partially enlarged section shown in Figure 5 is related to the operation stability of the non-smooth pressing roll. The smaller n_1 is, the larger the shadow part is, the more obvious the vibration of the press roller is, and vice versa. The reference is divided into two equal parts, and the dislocation angle is 22.5°. As shown in Figure 5, the non-smooth press roller is stable in operation and has a certain force reduction capability.

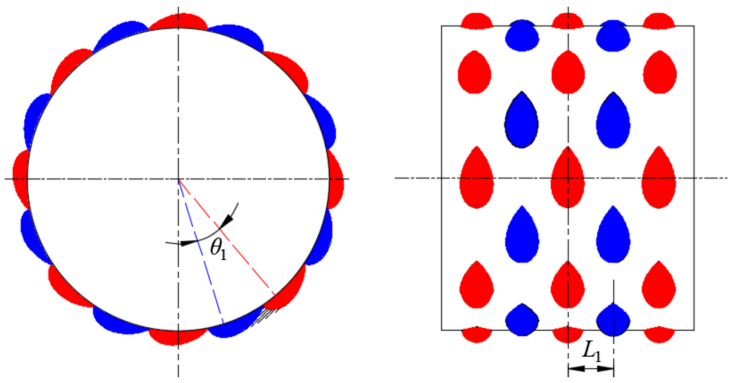

Figure 5. Definition of tine trajectory and parameters.

2.1.4. Axial spacing between adjacent radial base surfaces

The axial spacing between adjacent radial base surfaces is L_1, as shown in Figure 5. If its value is too large, the compaction effect is poor. If it is too small, too much compaction will affect the growth of wheat, and at the same time, the installation quantity and the operation cost will increase. It was preliminarily decided that the axial spacing, L_1, between adjacent radial basal planes is 30–50 mm.

2.1.5. Design of Bionic Press Roller

The convex hull geometry using UHMWPE [22,23] with viscosity reduction and anti-skid ability was fixed on the surface of a conventional smooth press roller by countersunk screws to realize the surface modification of the conventional smooth press roller. The specific structure is shown in Figure 6.

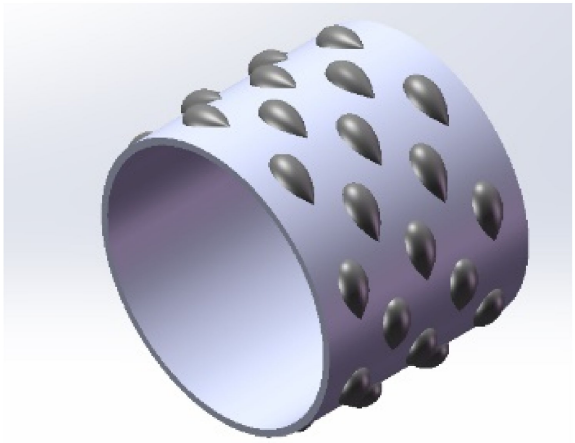

Figure 6. Bionic press roller.

2.2. Dynamic Simulation of Bionic Press Roller

Taking the bionic press roller as the research object, the explicit dynamics software ANSYS/LS-DYNA was used to establish the simulation model of the roller–soil interaction [24,25], which simulated the dynamic soil behavior of the bionic press roller in the field and provided methods and a basis for the subsequent performance design of the bionic press roller.

2.2.1. Simulation Model

The center base plane of the press roller and the adjacent base planes on both sides were selected as the simulation geometric prototype in Figure 7. The axial spacing was 40 mm. The structural model was fully hexahedrally meshed using HyperMesh 2020 software(Atair Engineering, Troy, Michigan, USA), as shown in Figure 7. The aspect radio was less than 5, and the Jacobian was more than 0.7 and less than 1. The MAT20 material model was selected as the press roller material. The elastic modulus, Poisson's ratio, and density were 2.1×10^5 MPa, 0.3, and 7800 kg/m^3, respectively.

The soil model in this paper adopted the special soil material model MAT193 (MAT_FHWA_SOIL) provided by LS_PREPOST (post-processing module of ANSYS/LS-DYNA software). The soil model was set as a simple cuboid with dimensions of 1.15 m × 0.3 m × 0.27 m (length × width × height). The elastic modulus, Poisson's ratio, density, and cohesive were 3.7 MPa, 0.3, 2031 kg/m^3, 0.8 kPa, respectively.

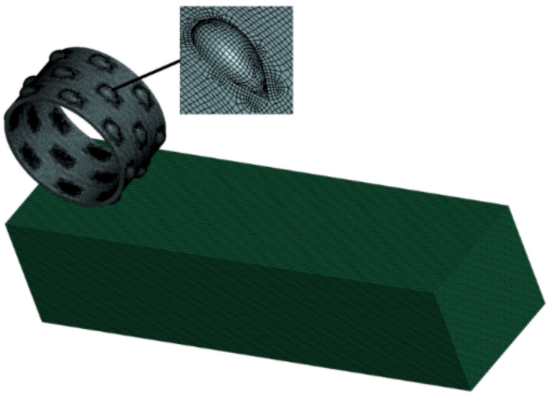

Figure 7. Finite element model of roller and soil.

2.2.2. Boundary Conditions

According to the actual working conditions of the cutter tooth, it rotated clockwise at a high speed around the central shaft and moved from right to left as the unit moved. During the numerical simulation, the added boundary conditions were as follows: (1) the forward speed of press roller was 3 km/h; (2) the load was 360 N; (3) the axial spacing was 40 mm; (4) we set the lowest degrees of freedom of the fully constrained soil model; (5) we set the rotational degrees of freedom, except the rotation of the roller model around the axis; (6) we set the degrees of freedom of lateral movement of the constrained press roller model; (7) the contact between the press roller and the soil was automatic surface-to-surface contact (contact-automatic-surface-to-surface); and (8) we set the solution time to 1 s. This study used LS_PREPOST to generate the K files, which were submitted to the MPP LS-DYNA R8 1.0 processor to solve and generate a solution report.

2.3. Analysis of Interaction between Roller and Soil

2.3.1. Interaction Models between Press Roller and Soil

The seedbed soil was loose before compaction. When working with the roller, the stress–strain relationship changes with time. There is a certain rheological property for the sticky soil in the rice–wheat rotation area under pressure, and its variation curve is similar to that of the Bergs model curve. Taking the paddy soil as the research object, the interaction models between the paddy soil and the roller were established, as shown in Figure 8.

$$\frac{\eta_1\eta_2}{E_2}\ddot{\varepsilon} + \eta_1\dot{\varepsilon} = \frac{\eta_1\eta_2}{E_1E_2}\ddot{\sigma} + (\frac{\eta_1}{E_1} + \frac{\eta_1}{E_2} + \frac{\eta_2}{E_2})\dot{\sigma} + \sigma \quad (3)$$

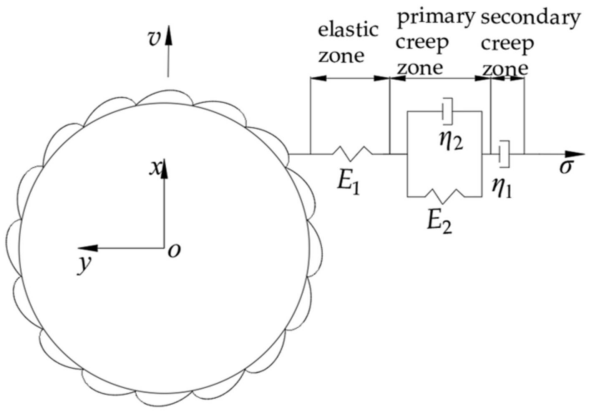

Figure 8. Model of the interaction between roller and soil (the direction of press roller movement is from down to up).

Laplace transform (8) to obtain

$$\varepsilon(s)\left(\frac{\eta_1\eta_2}{E_2}s^2+\eta_1 s\right)=\sigma(s)\left[\frac{\eta_1\eta_2}{E_1E_2}s^2+\left(\frac{\eta_1}{E_1}+\frac{\eta_1}{E_2}+\frac{\eta_2}{E_2}\right)s+1\right] \tag{4}$$

The unit step function $H(t)$ is used to describe the pressure property, namely,

$$p\cdot H(t)=\begin{cases}0 & t<0\\ 1 & t\geq 0\end{cases} \tag{5}$$

The form of the Laplace transform is p/s, according to the formula of sinkage

$$Z(s)=\frac{\alpha(1-\mu^2)}{\sqrt{A}D(s)}\cdot\frac{P}{s} \tag{6}$$

where A is the area; α is the shape correction factor; μ is Poisson's ratio; and $D(s)$ is the operator.

Then, by substituting Equations (5) and (6), Equation (7) can be obtained:

$$D(s)=\frac{\left(\frac{\eta_1\eta_2}{E_2}s^2+\eta_1 s\right)}{\left[\frac{\eta_1\eta_2}{E_1E_2}s^2+\left(\frac{\eta_1}{E_1}+\frac{\eta_1}{E_2}+\frac{\eta_2}{E_2}\right)s+1\right]} \tag{7}$$

Perform an inverse Laplace transform on Equation (7)

$$\mathrm{z}=0.0776P\left(a_1+a_2(1-e^{-a_3\cdot t})+a_4\cdot t\right) \tag{8}$$

where a_1, a_2, a_3, a_4 are the soil-related parameters.

According to the premise that the t (time) required for the roller to walk through the s (distance) with v (velocity) to sort out Equation (8), we can obtain Equation (9).

$$\mathrm{z}=0.0776P\left(a_1+a_2(1-e^{-a_3\cdot\frac{s}{v}})+a_4\cdot\frac{s}{v}\right) \tag{9}$$

It can be seen from Equation (9) that when the soil conditions are constant, the pressure and forward speed are the main factors affecting soil packing. The core of constructing a seedbed environment suitable for seed germination is to control the reasonable soil subsidence, so it is necessary to determine the combination of pressure and forward speed parameters through field tests.

2.3.2. Force Analysis of Bionic Convex Press Roller

Where the surface of the bionic press roller is working, there are two parts of the press roller and the soil: (1) the interaction between the soil and the bottom surface of press roller and (2) the interaction between the soil and the convex surface. Taking the press roller as the research object, a force analysis was carried out, as shown in Figure 9.

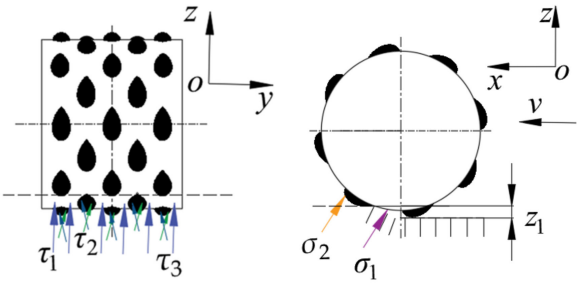

Figure 9. Sketch of forces on non-smooth press roller.

The total forces acting from the soil to the press roller consist of the sum of four three-dimensional vector forces: the normal and slide forces from the soil to the base circle surface of the press roller, F_{n1} and F_{f1}, and the normal and slide forces from the soil to the convex hull surface of the press roller, F_{n2} and F_{f2}. The forces are described by

$$\begin{cases} F_{n1} = \iint \sigma_1 \mathrm{d}A_1 \\ F_{n2} = \iint \sigma_2 \mathrm{d}n_2 A_2 \\ F_{f1} = \iint \tau_1 \mathrm{d}A_1 \\ F_{f2} = \iint \tau_2 \mathrm{d}\frac{n_2 A_2}{2} + \iint \tau_2 \mathrm{d}\frac{n_2 A_2}{2} \end{cases} \tag{10}$$

where σ_1 and σ_2 are the normal stress from the soil to the press roller; τ_1, τ_2, and τ_3 are the shear stress from the soil to the press roller, A_2 is the surface area of a single convex hull, n_2 is the constant of the convex hull in contact with soil, and A_1 is the contact area between the base circle and the soil.

A_1 is described by Equation (11).

$$A_1 = \arccos(\frac{R-z}{R})\frac{\pi R^2 d}{360} - n_2 \cdot A_3 \tag{11}$$

where d is the press convex roller width and R is the press convex roller radius.

Then, by substituting Equations (10) and (11), Equation (12) can be obtained:

$$\begin{cases} F_{n1} = (\arccos(\frac{R-z}{R})\frac{\pi R^2 d}{360} - n_2 \cdot A_3)\sigma_1 \\ F_{n2} = \sigma_2 n_2 A_2 \\ F_{f1} = (\arccos(\frac{R-z}{R})\frac{\pi R^2 d}{360} - n_2 \cdot A_3)\tau_1 \\ F_{f2} = (\tau_2 + \tau_3)\frac{n_2 A_2}{2} \end{cases} \tag{12}$$

The simplified Equation (12) in this paper considers the following three assumptions: first, the normal and shear stress are evenly distributed based on the isotropy of the soil material, thus $\sigma_1 = \sigma_2$ and $\tau_1 = \tau_2 = \tau_3$; second, the direction and amount of action of F_{n1} and F_{n2} are the same; and third, the slide force, F_{f2}, has zero component force along the x-axis. In the steady state, the total force, F_{sum}, acting from the soil to the press roller should be equivalent to the traction force, F_d, of which the resultant force, $\sum F_x$, along the x-axis is zero.

$$\sum F_x = F_d - F_{sum} = \arccos(\frac{R-z}{R})\frac{\pi R^2 d}{360}(\sigma_1 + \tau_1) + \sigma_1 n_2 (A_2 - A_3) \tag{13}$$

It can be seen in Equation (14) that when the other parameters are kept constant, the total force, F_{sum}, is positively correlated with the parameter n_2. When the press roller width is kept constant, the axial distance, L_1, is smaller and the n_2 is larger. Then, the total force, F_{sum}, is negatively correlated with the axial distance, L_1. Therefore, the axial distance, L_1, is a key factor of the bionic press roller, and the optimal value of the axial distance, L_1, should be determined through field tests.

2.4. Field Tests

2.4.1. Site Description

A field test was conducted in Lianyungang City, Jiangsu Province, China, during October 2021. The moisture content, dry bulk density, and penetration resistance of the 0–10 cm soil layer were 19.5 ± 1.3%, 1376 ± 32.3 kg/m^3, and 822 ± 110 kPa, respectively.

2.4.2. Experimental Design

To study the integrated influence of the structural and operational parameters on the bionic press roller, the orthogonal test design of three factors and three levels was used for the experiment. The treatments consisted of the combination of three forward speeds (3 km h^{-1}, 5 km h^{-1}, and 7 km h^{-1}), three loads (400 N, 600 N, and 800 N), and three axial

spacings (30 mm, 40 mm, and 50 mm),as shown in Table 1. Each test group was repeated three times. A total of 27 tests were conducted.

Table 1. Factor coding and experimental levels.

Factors	Spacing	Levels		
		1	**2**	**3**
Forward speed (km·h^{-1})	2	3	5	7
Load (N)	200	400	600	800
Axial spacing (mm)	10	30	40	50

2.4.3. Test Evaluation Index

The soil adhesion quality and the slip ratio were selected as the evaluation index, and the smaller the corresponding value, the better. The soil adhesion quality is a key factor that has great effect on the working performance of a press roller. The soil adhesion to the surface of the press roller was brushed off and collected using a brush, and its weight was measured using a digital balance. The slip ratio of the press wheel was defined as the ratio of the difference between the theoretical velocity and the actual velocity of the wheel and the theoretical velocity. The slip ratio can be expressed according to Equation (14).

$$\delta = 1 - \frac{\pi D n_3}{l} \tag{14}$$

where δ is the slip ratio, l is the test length, D is the press roller diameter, and n_3 is the number of wheel revolutions in the test length.

3. Results

3.1. Simulation Results

3.1.1. Stress Analysis

It can be seen from the simulation model of the bionic press roller in Figure 10 that the convex hull structures are arranged at equal intervals along the radial base surface, and the corresponding motion should be a periodic motion. In each cycle, according to the contact state between the convex hull and the soil, the interaction process between the convex hull structures and the soil was divided into five stages: no contact with the soil, partial contact with the soil, complete contact with the soil, partial separation from the soil, and complete separation from the soil, which correspond to time steps 22, 22, 24, 26, and 28, respectively. At different time steps, this section focuses on the analysis of the soil stress state in the above process.

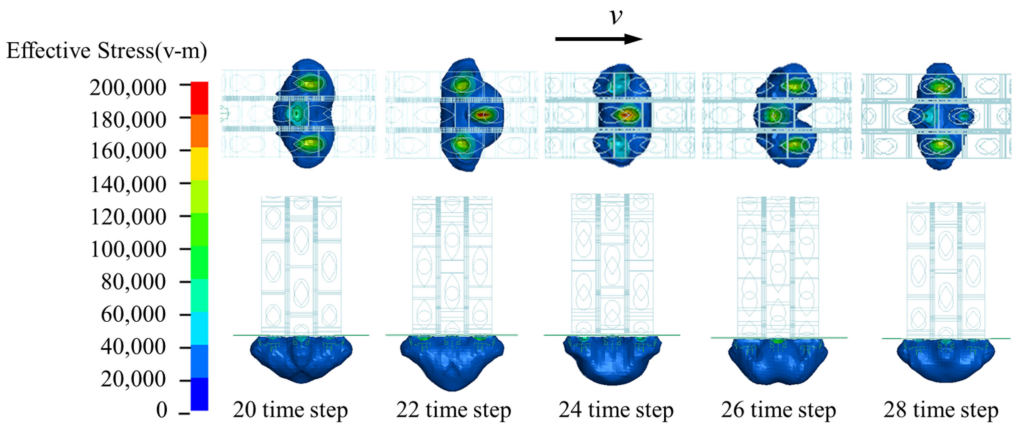

Figure 10. Stress change in stable stage (the direction of press roller movement is from left to right).

As shown in Figure 10, the soil stress field is constantly changing within time steps 22–28, and the soil stress fields corresponding to the time steps 20 and 28 are similar. The possibility of this phenomenon is the state in which the convex hulls on both sides are in complete contact with soil, corresponding to a similar degree of soil deformation. Compared with the other time steps, the time steps 22 and 24 have higher stress. At this time, the convex hull with the soil is bilateral and works together with the central convex hull to form a triangular stress superposition, which has a large overall deformation of the soil. The maximum stress field appears at time step 22. The convex hull on both sides is almost completely in the soil, and the convex hull part of the central base surface is in contact with the soil, which indicates that the convex hull on both sides has a greater impact on the stress field [26,27]. At time step 24, the convex hull of the central base surface is directly below the axis of rotation of the press roller, and the convex hull is in complete contact with the soil, which correspond to the largest stress and soil deformation in the direction of the central base. From time step 22 to 26, the overall stress field is in a medium convex state, which is an ideal stress field. It shows that the bionic pressing roller can increase the contact area between the seed and the soil, improve the seed germination ability, ensure the overwintering ability, and avoid the emergence of "bean sprout" seedlings in the rice–wheat rotation area.

3.1.2. Force Analysis

During the operation of a bionic press roller, the relationship between the working force of the press roller and time is shown in Figure 11. Within the time stage of 0–0.06 s, the bionic press roller performs a free fall movement under the action of gravity. In this process, the bionic press roller has no contact with the soil, and the corresponding three-dimensional force is 0. Within the time stage of 0.06–0.12 s, the bionic press roller makes a static pressure movement, and the forward force and vertical force first increase and then decrease, and finally reach stability. At 0.24 s, the forward speed and corresponding rolling speed are applied to the simulation model. After the time reaches 0.42 s, the bionic press roller enters the stable stage, and the three-dimensional force fluctuates within a certain range. Compared with the force in the period of 0.06–0.24 s, the absolute values of forward force and vertical force in the period of 0.42–0.78 s are relatively small as a whole, which indicates that there is a negative correlation between speed and force. The reason for this phenomenon may be that the faster the speed, the shorter the contact time with soil, and the lower the impact on soil deformation, the smaller the corresponding subsidence and the lower the operation force.

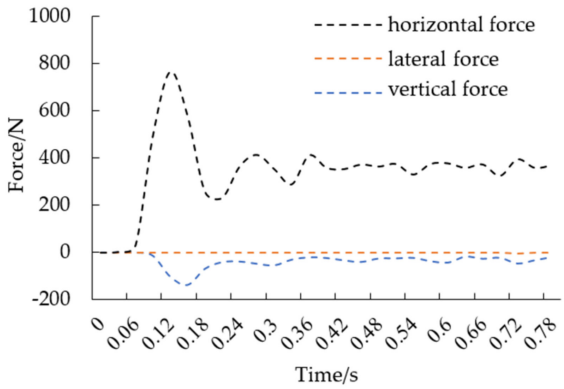

Figure 11. Three-axis working force curves of bionic press roller.

3.2. Results of Field Test

3.2.1. Effect of Experimental Factors on Working Performance

A range analysis was performed on the data in Table 2. According to the analysis results, the weight of the factors affecting the soil adhesion was $B > C > A$; the optimal levels of the factors were A_1, B_1, and C_2; and the optimal combination was $A_1B_1C_2$. Similarly, the

weight of the factors affecting the slip rate was $A > B > C$; the optimal levels of the factors were A_3, B_1, and C_2; and the optimal combination was $A_3B_1C_2$.

Table 2. Results of orthography experiment and range analysis.

No.		Factors			Soil Adhesion (g)	Slip Rate (%)
		A	*B*	*C*		
1		1	1	1	52.6	3.62
2		1	2	2	46.4	4.88
3		1	3	3	58.7	4.17
4		2	1	2	44.3	3.23
5		2	2	3	69.6	4.39
6		2	3	1	88.2	4.48
7		3	1	3	49.5	3.35
8		3	2	1	74.2	3.56
9		3	3	2	63.9	3.98
soil adhesion	k_1	52.57	48.80	71.67		
	k_2	67.37	63.40	51.53		
	k_3	62.53	70.27	59.27		
	R	14.80	21.47	20.14		
slip rate	k_1	4.04	3.63	3.89		
	k_2	4.44	4.22	3.79		
	k_3	3.40	4.03	4.21		
	R	1.047	0.592	0.413		

The mathematical statistics software SPSS 17 (IBM Corp., Armonk, NY, USA)was used to analyze the variance in the test results in Table 2 and to study the influence of the test factors on the evaluation indicators, as shown in Table 3.

Table 3. Variance analysis.

Index	Source	Sum of Squares	DF	Mean Square	*F* Value	*p* Value
soil adhesion	*A*	341.74	2	170.87	23.51	0.041 **
	B	721.13	2	360.56	49.61	0.020 **
	C	618.92	2	309.46	42.58	0.022 **
	Pure Error	14.54	2	7.27		
slip rate	*A*	1.67	2	0.84	71.12	0.014 **
	B	0.55	2	0.28	23.45	0.041 **
	C	0.28	2	0.14	12.00	0.077 *
	Pure Error	0.02	2	0.01		

note: "*" means relatively significant ($0.05 < p < 0.1$); "**" means significant ($0.01 < p < 0.05$).

It can be seen in Table 3 that in the indicators of soil adhesion, factors *A*, *B* and *C* were significant; in the slip ratio index, factors *A* and *B* were significant, and factor *C* was more significant; and the test factors had a significant impact on the evaluation index, which shows that the selection of test factors was reasonable and the test arrangement was appropriate. At the same time, it shows that the selection of forward speed, load, and axial spacing is very important for soil adhesion and the slip rate.

3.2.2. Comprehensive Optimization of Experimental Factors

Referring to the literature [28], the index data in Table 2 were standardized, and the data were comprehensively weighted according to the weight of soil adhesion amount of 0.4 and the weight of slip rate of 0.6. The results are shown in Table 4. The range results corresponding to the comprehensive score values are shown in Table 5. The smaller the overall score, the better.

Table 4. Value of comprehensive evaluation.

NO.	R_{1n}	R_{2n}	Y
1	−0.19	−0.21	−0.20
2	−0.33	0.56	0.20
3	−0.05	0.13	0.06
4	−0.38	−0.44	−0.42
5	0.20	0.26	0.24
6	0.62	0.32	0.44
7	−0.26	−0.37	−0.32
8	0.30	−0.24	−0.02
9	0.07	0.01	0.04

Table 5. Range analysis of comprehensive scores.

Comprehensive Weighted Value	A	B	C
k_1	0.02	−0.31	0.07
k_2	0.09	0.14	−0.06
k_3	−0.10	0.18	−0.01
R	0.12	0.49	0.08
Main and Secondary Factors		$A > B > C$	
Optimal level	A_3	B_1	C_2

The comprehensive score value of $A_3B_1C_2$ was the smallest, while the optimal parameter combination were selected as: forward speed 7 km/h, load 400 N, and axial spacing 40 mm, as shown in Table 5. The optimal axial spacing selected in this paper was 40 mm, and the corresponding geometric pattern of the press roller was the optimal geometric pattern.

3.2.3. Verification Test and Discussion

To verify the low-adhesion and low-slip characteristics of the designed bionic press roller, the bionic ridged press roller, commonly used by the wheat planter in the rice–wheat rotation area, was selected for the comparison experiment, as shown in Figure 12. Before the test, the optimal operation parameters of the bionic ridged press roller were screened to ensure that the bionic ridged press roller was in the optimal state for the comparison test. The test results are shown in Table 6.

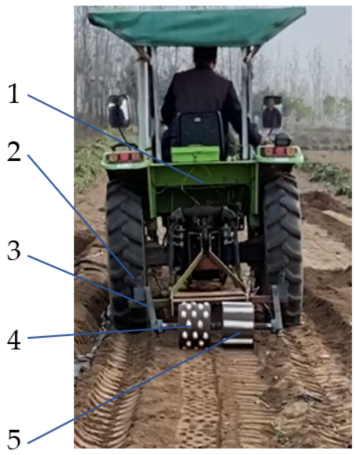

Figure 12. The scenario of verification test. 1. low-power tractor; 2. pressure control system; 3. profile control frame; 4. bionic convex press roller; 5. bionic ridged press roller.

Table 6. Working performance comparison of the bionic convex and bionic ridged press rollers.

Factors	Type of Press Roller	1	2	3	4	5	Average Value
Slip Rate (%)	Bionic ridged	6.75	7.26	5.18	6.72	6.58	6.50
	Bionic convex	2.58	2.51	2.42	2.31	2.37	2.44
Soil Adhesion (g)	Bionic ridged	72	80	85	96	75	82
	Bionic convex	35	43	45	39	39	40

As is shown in Table 6, the slip rate of the bionic press roller was 50% lower than that of the bionic ridged press roller, while the soil adhesion of the bionic press roller was 62% lower than that of the bionic ridged press roller. The possible reason for these phenomena is that the convex and concave state of the surface of the bionic press roller destroys the continuous water film between the soil and the surface of the press roller, which reduces the tangential force applied by the soil to the press roller and reduces the soil adhesion. Meanwhile, the structure of the convex hull increases the soil contact area and reduces the slip rate. In conclusion, the bionic press roller has the ability to reduce adhesion and resistance and has certain application value.

4. Conclusions

In this paper, a bionic press roller was designed based on the convex geometric characteristics of the back of *Carabus formosus nili*. By using the explicit dynamics software ANSYS/LS-DYNA, we found that the bionic press roller can increase the contact area between the seed and the soil, which was beneficial for wheat growth. In this paper, we found that forward speed, load, and axial spacing have significant influence on the soil adhesion and the slip rate, while the forward speed has the greatest impact on the soil adhesion and the slip rate. The best working parameters were a forward speed of 7 km/h, a load of 400 N, and an axial spacing of 40 mm for the rice–wheat rotation area in China. The findings of this paper showed that the bionic press roller can reduce the slip rate by 62.5% and reduce the soil adhesion by 51.2% compared with the bionic ridged press roller. The findings of this paper showed that the bionic press roller has a low-adhesion and anti-slip ability based on the geometric characteristics of the back of *Carabus formosus nili*. Therefore, this design method can be an effective means to provide future agricultural press roller designs.

In the future, two studies are necessary to verify and improve the working performance of the bionic convex press roller. First, future field tests should be conducted in very wet soil conditions with high straw contents, which are the most complex conditions in the rice–wheat rotation area. Second, the structure of the bionic convex press roller should continue to be improved with the micron-scale bionic morphology to reduce the soil adhesion.

Author Contributions: Conceptualization, H.L. and W.Z.; methodology, H.L.; software, W.Y.; validation, H.L. and W.Y.; investigation, Y.J.; data curation, W.Z.; writing—original draft preparation, H.L.; writing—review and editing, H.L. and Y.J.; supervision, W.Z. All authors have read and agreed to the published version of the manuscript.

Funding: This research was funded by the Natural Science Foundation of Jiangsu Province (Grant No. BE2020319-5) and the Central-Level Non-Profit Research Institutes Special Basic Research Expenses (Grant No. S202104-01).

Institutional Review Board Statement: Not applicable.

Informed Consent Statement: Not applicable.

Data Availability Statement: The datasets used and/or analyzed during the current study are available from the corresponding author on reasonable request.

Conflicts of Interest: The authors declare that they have no competing interest.

References

1. Zhu, H.; Li, H.; He, J.; Wang, Q.; Li, H.; Lu, C. No-till wheat seeder with two-axel drive anti-blocking in rice stubble field. *Trans. Chin. Soc. Agric. Mach.* **2013**, *44*, 39–44. [CrossRef]
2. Jiang, M.; Liu, C.; Wei, D.; Du, X.; Cai, P.; Song, J. Design and test of wide seedling strip wheat precision planter. *Trans. Chin. Soc. Agric. Mach.* **2019**, *50*, 53–62. [CrossRef]
3. Luo, W.; Gu, F.; Wu, F.; Xu, H.; Chen, Y.; Hu, Z. Design and experiment of wheat planter with straw crushing and inter-furrow collecting mulching under full amount of straw and root stubble cropland. *Trans. Chin. Soc. Agric. Mach.* **2019**, *50*, 42–52. [CrossRef]
4. Zhang, H.; Gu, F.; Wu, F.; Xu, H.; Gao, X.; Hu, Z. General situation and development on mechanized sowing of wheat after rice in Jiangsu Province. *J. Chin. Agric. Mech.* **2021**, *42*, 186–192. [CrossRef]
5. Li, B. *Agricultural Mechanics*; China Agricultural Mechanical Press: Beijing, China, 2003.
6. Jia, H.; Wang, W.; Wang, W.; Zheng, J.; Wang, Q.; Zhuang, J. Application of anti-adhesion structure based on earthworm motion characteristics. *Soil Tillage Res.* **2018**, *178*, 159–166. [CrossRef]
7. Wu, J.; Tang, Q.; Yuan, W.; Wang, S.; Wu, C. Design and parameter optimization of ditching and compacting parts of rapeseed carpet seedling transplanter. *Trans. Chin. Soc. Agric. Eng.* **2016**, *32*, 46–53. [CrossRef]
8. Zhang, S.; Zhao, W.; Dai, F.; Song, X.; Qu, J.; Zhang, F. Simulation analysis and test on suppression operation process of ridging and film covering machine with full-film double-furrow. *Trans. Chin. Soc. Agric. Eng.* **2020**, *36*, 20–30. [CrossRef]
9. Jia, H.; Wang, W.; Luo, X.; Zheng, J.; Guo, M.; Zhuang, J. Effects of profiling elastic press roller on seedbed properties and soybean emergence under double row ridge cultivation. *Soil Tillage Res.* **2016**, *162*, 34–40. [CrossRef]
10. Jia, H.; Jiang, X.; Guo, M.; Zhao, J.; Wang, F.; Wang, L. Design and experiment of type 2BH-3 inter-row seeder. *Trans. Chin. Soc. Agric. Mach.* **2015**, *46*, 83–89. [CrossRef]
11. Tong, J.; Zhang, Q.; Guo, L.; Chang, Y.; Guo, Y.; Zhu, F.; Chen, D.; Liu, X. Compaction performance of biomimetic press roller to soil. *Biosys. Eng.* **2015**, *12*, 152–159. [CrossRef]
12. Wang, J. *The Research of Position Control after Seed Contacting Soil in the Process of Soil Covering and Rolling with Precision Seeder*; Jilin University: Changchun, China, 2014.
13. Wang, W. *Bionic Press Device with Profiling Mechanism for Soybean Precision Planter*; Jilin University: Changchun, China, 2016.
14. Acquah, K.; Chen, Y. Soil compaction from wheel traffic under three tillage systems. *Agriculture* **2022**, *12*, 219. [CrossRef]
15. Jia, H.; Wang, W.; Zhuang, J.; Luo, X.; Yao, P.; Li, Y. Design and experiment of profiling elastic press roller. *Trans. Chin. Soc. Agric. Mach.* **2015**, *46*, 28–34, 83. [CrossRef]
16. Zhang, Q. *Soil Press Roller with Bionically Geometrically Structured Surfaces*; Jilin University: Changchun, China, 2014.
17. Tong, J.; Zhang, Q.; Chang, Y.; Chen, D.; Dong, W.; Zhang, L. Reduction of soil adhesion and traction resistance of ridged bionic press rollers. *Trans. Chin. Soc. Agric. Mach.* **2014**, *45*, 135–140. [CrossRef]
18. Chang, Y. *Bionic Soil Press Roller with Convex Geometrical Structure*; Jilin University: Changchun, China, 2014.
19. Guo, H. *Research and Experiment of Elastic Press Device for Inter-Row Till-Planter*; Jilin University: Changchun, China, 2014.
20. Zhao, J. *Research of Key Technology of No-Tillage Seeder for Stubble Retain with Alternating Tillage*; Jilin University: Changchun, China, 2015.
21. Shen, T. *Biology and Artificial Rearing of Carabus Formosus Nili from Shaanxi Province*; Northwest A&F University: Yangling, China, 2010.
22. Adisa, A.F.; Eberendu, N.O.; Aderinlewo, A.A.; Kuye, I.S. Effectiveness of Teflon as roller material for a prototype rice processing machine. *Agri. Eng. Int. CIGR J.* **2016**, *18*, 107–118.
23. Zhang, Z. *Interaction of Soil and Rolling Soil Engaging Components for Micro-Topographical Preparation and Their Bionic Geometrical Structures*; Jilin University: Changchun, China, 2014.
24. Ozakia, S.; Hinata, K.; Senatore, C.; Iagnemma, K. Finite element analysis of periodic ripple formation under rigid wheels. *J. Terramechanics* **2015**, *61*, 11–22. [CrossRef]
25. Zhou, W.; Sun, X.; Liu, Z.; Qi, X.; Jiang, D.; Wang, J. Simulation analysis and test of interaction between pricking hole needle body of liquid fertilizer hole applicator and soil. *Trans. Chin. Soc. Agric. Mach.* **2020**, *51*, 87–94. [CrossRef]
26. Kurjenluoma, J.; Alakukku, L.; Ahokas, J. Rolling resistance and rut formation by implement tyres on tilled clay soil. *J. Terramechanics* **2009**, *46*, 267–275. [CrossRef]
27. McKyes, E. *Soil Cutting and Tillage*; Developments in Agricultural Engineering; Elsevier: Amsterdam, The Netherlands, 1989.
28. Liu, H.; Zhao, S.; Tan, H.; Yang, Y.; Zhang, X. Investigation on press device in reducing adhesion and resistance based on scrape and vibration principle. *Trans. Chin. Soc. Agric. Mach.* **2018**, *49*, 86–92. [CrossRef]